# Solvent-free production of carbon materials with developed pore structure from biomass for high-performance supercapacitors

Lang Huang a,b, Qiong Wua,b,c, \*, Shouxin Liub, Shitao Yua, \*, Arthur J. Ragauskasc

- <sup>a</sup> State Key Laboratory Base of Eco-Chemical Engineering, College of Chemical Engineering, Qingdao University of Science and Technology, 53 Zhengzhou Road, Qingdao, Shandong Province, 266042, PR China
- <sup>b</sup> College of Materials Science and Engineering, Northeast Forestry University, Harbin, 150040, PR China
- <sup>c</sup> Joint Institute of Biological Science, Biosciences Division, Oak Ridge National Laboratory, Oak Ridge, TN, 37830, USA
- □ Corresponding authors at: State key laboratory base of eco-chemical Engineering, College of Chemical Engineering, Qingdao University of Science and Technology, 53 Zhengzhou Road, Qingdao, Shandong province, 266042, PR China. E-mail addresses: wuqiong0506@hotmail.com (Q. Wu), yushitaoqust@126.com (S. Yu).

## **ABSTRACT**

The study aimed at preparing porous carbon materials, with superhydrophilic characteristics and developed micro/mesoporous structure (CSB-800), from corn stover by a solvent-free method including pre-carbonization, ball milling, and activation. The effect of pre-carbonization, ball milling on the detailed structural composition and properties especially the hydrophilicity and porous structures were studied, and the potential application of CSB-800 as electrode in supercapacitors was also investigated. The results revealed that pre-carbonization increased the accessibility of raw materials as well as the efficiency of the ball milling with KOH, leading to small carbon particles with good dispersion behavior. Ball milling promoted the porosity, surface energy, hydrophilicity, crystallinity, and graphitization of the carbon materials. CSB-800 exhibited a high specific surface area of 2440.6 m² /g with developed micro and porous structures. The heteroatom nitrogen formed nitrogen-containing groups of N-Q and N-X, which provided faradaic pseudocapacitance when CSB-800 was used as an electrode material, and this material presented a specific capacitance of 398 F/g at 0.5 A/g in 1 M H<sub>2</sub>SO4 electrolyte in a three-electrode system,

while the value was 243 F/g in a two-electrode system, and the energy density reached 5.01 Wh/kg at a power density of 100 W/kg.

#### 1. INTRODUCTION

Porous carbon materials attract increasing attentions recent years due to their advantages such as abundant pore structure, adjustable pore diameters, and high heat resistance (Lee et al., 2006). In particular, microporous carbon materials, which possess large specific surface areas and highly ordered crystalline structure, present high stability and have been widely applied in fields including separation and catalysis, but their small pore sizes become the main obstacle limiting the passage of many macromolecules (Liu et al., 2016). In contrast, mesoporous carbon materials generally have moderate pore size that can be adjusted within a certain range, making them suitable for drug carrier and energy storage applications, but the simple mesoporous structure usually exhibits poor stability (Jin et al., 2010; Wu et al., 2014). To overcome the above-mentioned deficiencies of the simple microporous or mesoporous structures, a combination of micro- and mesoporous structures was proposed recently to achieve the synergistic benefits.

Various porous carbon materials with adjustable pore sizes which obtained from biomass-based raw materials including watermelon or grapefruit peels and straws (Huang et al., 2017; Li et al., 2018), display improved performance in energy storage, adsorption, and medical applications when compared with those of the traditional petroleumbased carbon materials (Maria-Magdalena Titirici and Antonietti, 2010). Biomass-derived carbon materials pose a large number of oxygen-containing groups on the surface, which makes it easy for tailored modifications and functionalizations (Danish and Ahmad, 2018; Xiao et al., 2012). However, most such carbon

materials possess low surface energy and hydrophobic feature, which directly affect their performance and limit their use in applications with water as the solvent (Tan et al., 2018). Besides, the porous structures of such materials without additional treatments are usually disordered and undeveloped, which need to be resolved for expanded applications.

Traditional methods to prepare biomass-derived carbon materials including hydrothermal carbonization, direct carbonization, and pyrolysis (Thines et al., 2017; Wu et al., 2015) tend to cause material agglomerations during the reaction in the dry or solvated state, because of the long reaction time. In addition, the obtained materials are hardly dispersed effectively during processing, leading to poor mechanical properties and surface energy and limiting their use in high-value applications. Unlike traditional solution approaches requiring dissolution, heating, and stirring, mechanochemical reactions uses small amount or no solvent to break chemical bonds on the surface through high-energy collisions, and the generated free ions and/or unsaturated bonds increase the internal energy, chemical reaction equilibrium constant, and reaction rate (Tang et al., 2013). As a green mechanochemical method with high energy efficiency, ball milling is widely used in materials and chemistry fields. During the ball milling process, a lot of collisions between the milling ball/inner chamber wall and the charged materials occurred, producing strong shearing and compressing forces to break down the charged carbon material and reduce the particle size. With the grinding, mechanical energy could directly rupture the ordered crystal structure and influence the surface property, leading to increased specific surface area and promoting the particle porosity regulation.

Here in this work, a solvent-free method-ball milling was used to prepare porous carbon materials with superhydrophilic characteristics from corn stover. The effect of pre-carbonization, ball milling on the detailed structural composition and structural properties were studied, the

potential application of the as prepared porous carbon in supercapacitors was also investigated. This study presents an effective route to prepare superhydrophilic porous carbon with excellent electrochemical performance and the results obtained are of great importance to shed light on the multifunctional applications of the as-prepared carbon in the environmental and energy fields.

#### 2. EXPERIMENTAL SECTION

## 2.1. Preparation of porous carbon materials

The raw material corn stover (40–80 mesh) was collected from a factory in Shandong, China and its main components are listed in Table S1. Before use, the corn stover was dried to constant weight. A certain amount of the corn stover powder was placed in a quartz boat and then heated to 500 °C under N<sub>2</sub> protection for 2 h. The obtained product (labeled as CSpre) was mixed with KOH (mass ratio 1:3) and ball milled for 2 h at 600 rpm. The obtained product was then heated to 700, 800, or 900 °C for 2 h under N<sub>2</sub> atmosphere. The obtained product (CSB-T, where T represents the carbonization temperature) was washed with 1 M HCl and distilled water until the solution was neutral before being dried at 100 °C overnight. For comparison, reference sample without pre-carbonization but with ball milling was denoted as CB-T, reference sample without ball milling but with pre-carbonization was denoted as CS-T.

## 2.2. Surface energy calculation

Contact angles of carbon materials were measured on a contact angle system (DSA25, Kruss, Hamburg, Germany) at room temperature using a droplet volume of 5  $\mu$ L. Two polar liquids

(water and formamide (99.5 %)) and one apolar liquid (diiodomethane (99 %)) were used for determination of the surface energy based on previous literature (Van Oss, 2006).

### 2.3. Characterization

Elemental analysis was conducted on EA3000 analyzer (Euro Vector, Italy). A thermogravimetric analyzer (TGA, Netzsch, Germany) was used to analyze the heating behavior and ash content of samples in both  $N_2$  and air atmospheres. Microstructures and morphology investigations of the samples were observed by scanning electron microscopy (SEM; Hitachi S4800, Japan) and transmission electron microscopy (TEM; JEOL 2011, Japan). Raman spectra were performed on a Raman spectrometer with 514-nm argon-ion laser excitation (InVia, Renishaw, UK). X-ray diffraction (XRD, Japan) characterization was tested using Rigaku D/Max-rB diffractometer in the range of 5°–50°. X-ray photoelectron spectroscopy (XPS) analysis was conducted on PHI5700 spectrometer with Al-K $\alpha$  radiation (hv =1486.6 eV) (Chanhassen, USA). Pore structure was characterized using  $N_2$  adsorption—desorption isotherm measurements at -196°C (ASAP 2020, Micromeritics, USA), Brunauer–Emmett–Teller (BET) and density functional theory (DFT) was used to calculate the specific surface area and pore size distribution of the samples.

## 2.4. Electrochemical testing

Three and two-electrode systems were assembled for electrochemical tests as detailed in our previous work (Wu et al., 2019). All the characterization tests in this study have been replicated three times.

## 3. RESULTS AND DISCUSSION

SEM and TEM images were used to reveal the macroscopic and microscopic morphologies of CSB-800, CB-800, and CS-800 as shown in Fig. 1(a–h). The sample subjected to pre-carbonization and ball milling (CSB-800) consisted of well-dispersed particles with diameters of 1–5 μm, while those without pre-carbonization (CB-800; Fig. 1(c and d)) presented to be large blocks (> 10 μm in diameter) without a specific morphology. Some fragments and crystalline structure were observed in the TEM images, which may be derived from ball milling directly destroying the fibers. The CS-800 sample consisted of much larger particles that retained the original structure of corn stover. These results revealed that ball milling decreased the size of the solid particles during grinding through mechanochemical reactions. Pre-carbonization increased the effectiveness of ball milling to yield carbon particles with small diameter, uniform morphology, and narrow size distribution.

Some short-range ordered lattice structures with a lattice spacing of 0.34 nm were observed for CSB-800, as shown in Fig. 1(g) and (h), which was consistent with graphite-like structure (Liu et al., 2019). Some disordered porous structure was also seen in CSB-800. Elemental mapping (Fig. 1(I)) was used to reveal element composition and distributions in the samples. The mapping of CSB-800 indicated the presence of C, O, N, and S in the porous structure. Both N and S atoms were homogeneously distributed in CSB-900, indicating that this sample was an N/S co-doped porous carbon material.

The contact angle of the samples prepared with and without precarbonization and ball milling were measured to investigate their surface characteristics. As presented in Figs. S1 and

1(J). The CS<sub>pre</sub> sample exhibited a contact angle of 148.8°, which demonstrated the hydrophobicity of the obtained material. In contrast, the samples after ball milling showed hydrophilic nature with contact angles of smaller than 20°. The CB-800 sample was also hydrophilic, whereas that of CS-800, the sample produced without ball milling, was 75.2°. Although lower than that of CS<sub>pre</sub>, the hydrophilic character of CS-800 was far weaker than that of CSB-800. These results indicated that ball milling directly influences the hydrophilic/phobic character of the obtained carbon materials, and also indicating that ball milling can grind the starting material into much smaller particles, which helps the carbon material to effectively contact KOH during the activation process. In addition, the energy generated during ball milling in the presence of KOH could change the surface energy of the carbon material, which effectively improves its wettability.

Surface energies of the samples were calculated as displayed in Fig. 1(J). Both the dispersive and polar components of CSB-800 were higher than those of CS-800. As a result, the total surface energy of CSB800 reached 51.5 mJ/m<sup>2</sup>. Such a high surface energy verified the above conclusion that ball milling can raise the surface energy of carbon materials (Li et al., 2013).

Raman analysis was carried out to investigate the structure especially the degree of order of obtained samples as shown in Fig. 2(a). All samples displayed two characteristic peaks centered at around 1350 and 1590 cm<sup>-1</sup>, corresponding to the D and G bands, respectively. The D band originates from defective and disordered carbon and the G band is related to the interlayer vibration of graphitic carbon (Wu et al., 2019). The intensity ratio of the D band to the G band (ID/IG) for each sample was obtained by integrating the peak areas, as listed in Table 1. ID/IG was 1.92 for CS-800, 1.69 for CB-800, and 1.66 for CSB-800.

Although all the samples consisted of carbon that was mostly amorphous with a certain degree of graphitization, the decrease of ID/IG for CB-800 and CSB-800 indicated that ball milling effectively increased the degree of graphitization of the samples.

XRD patterns of the samples are depicted in Fig. 2(b) to further describe the carbon crystal structure. There is a broad peak centered at 22.5° for CS<sub>pre</sub>, which was ascribed to amorphous carbon structure. This peak shifted to 24.5° for CSB-800, corresponding to the 002 lattice spacing (Xia and Mokaya, 2004). The calculated d-spacing for CSB-800 was 0.34 nm, indicating the crystallinity and graphitization degree of the samples increased after ball milling (Li et al., 2017). The broad peak only shifted to 23.1° for CS-800, indicating that this sample contained a higher content of amorphous structure than that for CBS-800. Overall, the XRD results illustrate that ball milling can be beneficial to form carbon materials with a high degree of graphitization.

XPS analysis was then conducted to reveal the detailed surface chemistry and functional groups of the samples. C, O, N, and S were detected in the samples; detailed composition data is given in Table 1. The surface of CSB-800 contained 4.6 % S and 9.2 % N, which are higher than those for CS-800 and CB-800, suggesting that pre-carbonization and the followed ball milling can promote stable heteroatom doping of carbon materials. Fig. 2(c) presents high-resolution C1s spectra of the samples. Functional groups such as C-C (284.8 eV), C-O (285.7 eV), C=O (286.9 eV), and O-C=O (288.5 eV) were observed, indicating the abundant oxygen-containing groups on the sample surfaces. A satellite peak at 290.2 eV corresponding to  $\pi$ - $\pi$ \* transitions was also detected, indicating the existence of the graphene-like microstructure (Shi et al., 2017). The high-resolution N1s spectra in Fig. 2(d) were able to be deconvoluted into three peaks originating from pyridine and pyridone (400.2 eV; N-5), quaternary N (401.8 eV; NeQ), and pyridine-N-oxide (402.6 eV; NeX), which are the main N-containing groups and are all stable (Seredych et al., 2008).

The presence of N can help to enhance the conductivity and capacitance of carbon materials. The high-resolution S2p spectra revealed that  $SO_X$  was the main sulfurcontaining functional group. In addition, CSB-800 exhibited the lowest ash content and highest residual carbon content of the samples. These results all indicated that ball milling is an efficient approach to prepare functional carbon materials.

To examine the effects of pre-carbonization, ball milling, and activation on the pore structure,  $N_2$  adsorption-desorption isotherms for CSB-800, CB-800, and CS-800 were tested and illustrated in Fig. 2(f). All the samples exhibited type IV and I isotherms, which indicated the presence of both meso- and micropores (Suryavanshi et al., 2012). The corresponding textural parameters of the samples derived from the  $N_2$  adsorption/desorption isotherms are summarized in Table 2. The specific surface area of CB-800 was 1032 m²/g and mesopores accounted for 78.48% of the porous structure. CSB-800 exhibited the most developed porous structure of the samples, with the highest specific surface area of 2441 m²/g and Smicro of 1514 m²/g. This was because precarbonization helped to increase the contact of the carbon precursor with KOH during subsequent ball milling, promoting the formation of microporous structure. CS-800 had a specific surface area of 1646 m²/g and both  $S_{meso}$  and  $S_{micro}$  were lower than those of CSB-800. This may be attributed to that ball milling decreases the particle size, which promotes effective contact with KOH and the formation of both mesoporous and microporous structures.

The pore size distributions of the sample were calculated using DFT method (Fig. 2(g)). The pore sizes were centered around 1.0–2.0 nm for both CSB-800 and CS-800, further verifying the existence of micropores in these two samples, and based on the data of pore volume, ball milling can further introduce micropores. The pore sizes of CB-800 were mainly centered at 1.0–

2.0 and 2.0–4.0 nm, indicating that ball milling without pre-carbonization can aid the formation of mesopores.

The  $N_2$  adsorption/desorption isotherms for CSB-700, CSB-800, and CSB-900 are shown in Fig. S2 and corresponding parameters are listed in Table S2. With rising carbonization temperature, the specific surface area increased from 1924 to 3147 m<sup>2</sup>/g and both  $S_{micro}$  and  $S_{meso}$  increased. For CSB-900, mesoporous structure was dominant, accounting more than 92 % of the pores. The pore diameter distributions indicate that activation at high temperatures caused the microporous structure to collapse to form a large number of mesopores. Considering the overall properties of the samples, CSB-800 was chosen for use in further experiments.

Based on the above characterization results, the structure evolution of corn stover during pre-carbonization, ball milling, and activation/ carbonization depicted in Fig. 3 was proposed. Corn stover contains cellulose as the skeleton structure along with hemicellulose and lignin. After pre-carbonization, the components were all carbonized but still maintained the original skeleton structure. At this stage, the carbon precursor was amorphous with low accessibility and relatively low carbon content. When this precursor was mixed with KOH and ball milled, the grinding impact of the beads caused the carbon precursor to mix effectively with KOH, leading to the formation of particles with relatively small and uniform diameters; at the same time, the output power of ball milling increased the surface energy of the carbon material.

During the activation process, KOH reacted with the carbon precursor to form K<sub>2</sub>CO<sub>3</sub> (Lillo-Ródenas et al., 2004). During the subsequent carbonization process, K<sub>2</sub>CO<sub>3</sub> reacted with carbon, forming numerous micropores and mesopores. K<sub>2</sub>CO<sub>3</sub> can also degrade and induce additional activation via gasification, resulting in some graphenelike edges (Wang et al., 2015). At

the same time, metallic K can contribute to rearrangement of amorphous carbon at 800 °C (Shi et al.,

2017), thus the superhydrophilic porous carbon materials with developed micropores and some ordered mesopores were obtained.

The performance of CSB-800, CS-800, and CB-800 as supercapacitors electrode materials in a three-electrode system with 1 M H<sub>2</sub>SO<sub>4</sub> electrolyte was tested, as shown in Fig. 4, to evaluate their potential as electrode material. The CV curves of all the samples were rectangular at lower scan rates, indicating ideal double-layer capacitance. Obvious peaks were observed in the range of 0.2–0.6 V (Fig. 4(a), (c), and (e)), which were attributed to redox reactions of N- and Ocontaining functional groups (Wang et al., 2012). CSB-800 exhibited the highest profile of the redox peak due to it contained the most N and S of the samples. The faradaic pseudocapacitance increased the specific capacitance of all electrodes. The specific capacitances of CSB-800, CS800, and CB-800 calculated from GCD curves were 398, 295, and 172 F/g at 0.5 A/g, respectively, in 1 M H<sub>2</sub>SO<sub>4</sub> electrolyte. These values are higher than those of many traditional carbon materials (Lei et al., 2018; Yu et al., 2017). Functional groups such as N-5 and oxygen-based groups possess electrochemical activity that contributes to faradaic pseudocapacitance in acid electrolyte. Meanwhile, N-Q and N-X groups can accelerate the electron transfer rate, decrease the internal resistance, and increase the electrical conductivity of the system, leading to high specific capacitance (Li et al., 2015). The outstanding performance of CSB-800 could also be attributed to its superhydrophilic surface and developed micro/mesoporous structure due to the pore structure could facilitate the contact between the active material and electrolyte.

Electrochemical impedance spectroscopy at an open circuit potential was further measured to evaluate the performances of CB-800, CS800 and CSB-800, and the obtained Nyquist plots are

shown in Fig. 4(g). All the samples exhibited straight lines at low frequency and small circles at high frequency. The equivalent series resistances for CS800 and CB-800 were 1.06 and 1.21  $\Omega$ , respectively, whereas it was only 0.92  $\Omega$  for CSB-800 because of its superhydrophilic character and developed microporous structures. The low resistance of CSB-800 leads to high conductivity, facilitating high supercapacitive performance. After 10,000 cycles at a current density of 20 A/g (Fig. 4(h)), CSB-800 and CB-800 displayed almost no capacity loss, confirming the high stability of the samples obtained by ball milling.

To further evaluate the electrochemical performance of CSB-800, a two-electrode test was conducted in 1 M  $_2SO_4$  electrolyte, as shown in Fig. 5. A relatively reversible rectangular profile was obtained at a scan rate of 50 mV/s. The charge/discharge curves are highly linear and symmetrical, indicating excellent electric double layer behavior. From the triangular charge/discharge curves, the specific capacitance was calculated to be 243 F/g at 0.5 A/g and 170 F/g at a current density of 10 A/g (Fig. 5(c)). EIS analysis (Fig. 5(d)) revealed that the charge transfer resistance (diameter of the semicircle) of CSB-800 was only 0.4  $\Omega$ , indicating its low ion diffusion resistance and electrical resistance, which contribute to its excellent capacitive properties. Capacitance retention tests were performed at 20 A/g for 10,000 cycles (Fig. 5(e)); over 80 % capacitance retention was observed after 10,000 cycles. Furthermore, the energy density of CSB-800 was 5.01 Wh/kg at a power density of 100 W/kg in 1 M  $_2SO_4$  electrolyte, and its energy density still reached 2.74 Wh/kg when the power density was increased to 10,000 W/kg.

#### 4. CONCLUSIONS

This study developed a solvent-free route involving pre-carbonization, ball milling, and carbonization to prepare superhydrophilic porous carbon materials with well-developed microporous structures. Ball milling ground the raw materials into small particles, which promoted their mixing and activation with KOH to form a superhydrophilic material with high surface energy. Pre-carbonization helped to make ball milling more effective and the obtained carbon materials dispersed more evenly than those without pre-carbonization. Pre-carbonization and ball milling together had a synergistic effect on the preparation of carbon materials. CSB-800 possessed high surface area, developed micro/mesoporous structure, and N-X, N-Q, and SO<sub>X</sub> functional groups. The developed porous structure and surface functional groups of CSB-800 improved its electrochemical performance as an electrode material. The developed pore structure promoted mass transfer of the electrolyte, while N-X and N-Q groups increased both electrical conductivity and wettability. As a result, in a three-electrode system with 1 M H<sub>2</sub>SO<sub>4</sub> as the electrolyte, CSB-800 exhibited a specific capacity of 398 F/g at 0.5 A/g, which was higher than those of CS-800 and CB-800. Overall, this study presents an effective route to prepare superhydrophilic carbon materials with excellent electrochemical performance.

#### CREDIT AUTHORSHIP CONTRIBUTION STATEMENT

Lang Huang: Data curation, Formal analysis. Qiong Wu: Writing - original draft. Shouxin Liu: Supervision. Shitao Yu: Funding acquisition. Arthur J. Ragauskas: Writing - review & editing.

#### DECLARATION OF COMPETING INTEREST

The authors declare that they have no known competing financial interests or personal relationships that could have appeared to influence the work reported in this paper.

## **ACKNOWLEDGMENTS**

Key Laboratory of Bio-based Material Science & Technology (Northeast Forestry University), Ministry of Education (SWZMS201901), the National Natural Science Foundation of China (31700517), Qingdao Applied Basic Research Program (18-2-2-4-jch), China Postdoctoral Science Foundation (2019M652504) and the Taishan Scholars Program of Shandong Province (ts201511033) financially supported this work.

#### APPENDIX A. SUPPLEMENTARY DATA

Supplementary material related to this article can be found, in the online version, at doi:https://doi.org/10.1016/j.indcrop.2020.112384.

## REFERENCES

Danish, M., Ahmad, T., 2018. A review on utilization of wood biomass as a sustainable precursor for activated carbon production and application. Renew. Sustain. Energy Rev. 87, 1–21.

Huang, B.B., Liu, Y.C., Xie, Z.L., 2017. Biomass derived 2D carbons via a hydrothermal carbonization method as efficient bifunctional ORR/HER electrocatalysts. J. Mater. Chem. A 5, 23481–23488. https://doi.org/10.1039/C7TA08052B.

Jin, J., Tanaka, S., Egashira, Y., Nishiyama, N., 2010. KOH activation of ordered mesoporous carbons prepared by a soft-templating method and their enhanced electrochemical properties.

Carbon 48, 1985–1989. https://doi.org/10.1016/j.carbon.2010.02.005.

Lee, J., Kim, J., Hyeon, T., 2006. Recent progress in the synthesis of porous carbon materials. Adv. Mater. 18, 2073–2094. https://doi.org/10.1002/adma.200501576.

Lei, E., Li, W., Ma, C.H., Xu, Z., Liu, S.X., 2018. CO2-activated porous self-templated N-doped carbon aerogel derived from banana for high-performance supercapacitors. Appl. Surf. Sci. 457, 477–486. https://doi.org/10.1016/j.apsusc.2018.07.001.

Li, F., Biagioni, P., Bollani, M., Maccagnan, A., Piergiovanni, L., 2013. Multi-functional coating of cellulose nanocrystals for flexible packaging applications. Cellulose 20, 2491–2504. https://doi.org/10.1007/s10570-013-0015-3.

Li, Y., Lu, C.X., Zhang, S.C., Su, F.Y., Shen, W.Z., Zhou, P.C., Ma, C.L., 2015. Nitrogen-and oxygen-enriched 3D hierarchical porous carbon fibers: Synthesis and superior supercapacity. J. Mater. Chem. A 3, 14817–14825. https://doi.org/10.1039/C5TA02702K.

Li, Z.S., Zhang, L., Li, B.L., Liu, Z.S., Liu, Z.H., Wang, H.Q., Li, Q.Y., 2017. Convenient and large-scale synthesis of hollow graphene-like nanocages for electrochemical supercapacitor application. Chem. Eng. J. 313, 1242–1250. https://doi.org/10.1016/j.cej.2016.11.018.

Li, S.C., Hu, B.C., Ding, Y.W., Liang, H.W., Li, C., Yu, Z.Y., Wu, Z.Y., Chen, W.S., Yu, S.H., 2018. Wood-derived ultrathin carbon nanofiber aerogels. Angew. Chem. Int. Ed. 57, 7085–7090. https://doi.org/10.1002/anie.201802753.

Lillo-Ródenas, M.A., Juan-Juan, J., Cazorla-Amorós, D., Linares-Solano, A., 2004. About reactions occurring during chemical activation with hydroxides. Carbon 42, 1371–1375. https://doi.org/10.1016/j.carbon.2004.01.008.

Liu, Y., Li, K., Ge, B., Pu, L., Liu, Z., 2016. Influence of micropore and mesoporous in activated carbon air-cathode catalysts on oxygen reduction reaction in microbial fuel cells. Electrochim. Acta 214, 110–118. https://doi.org/10.1016/j.electacta.2016.08.034.

Liu, C.F., Liu, Y.C., Yi, T.Y., Hu, C.C., 2019. Carbon materials for high-voltage supercapacitors. Carbon 145, 529–548. https://doi.org/10.1016/j.carbon.2018.12.009.

Maria-Magdalena Titirici, M.M., Antonietti, M., 2010. Chemistry and materials options of sustainable carbon materials made by hydrothermal carbonization. Chem. Soc. Rev. 39, 103–116.

Seredych, M., Hulicova-Jurcakova, D., Lu, G.Q., Bandosz, T.J., 2008. Surface functional groups of carbons and the effects of their chemical character, density and accessibility to ions on electrochemical performance. Carbon 46, 1475–1488.

https://doi.org/10.1016/j.carbon.2008.06.027.

Shi, C., Hu, L.T., Guo, K., Li, H.Q., Zhai, T.Y., 2017. Highly porous carbon with graphene nanoplatelet microstructure derived from biomass waste for high-performance supercapacitors in universal electrolyte. Adv. Sustain. Syst. 1, 1600011–1600020.

https://doi.org/10.1002/adsu.201600011.

Suryavanshi, U., Iijima, T., Hayashi, A., Hayashi, Y., Tanemura, M., 2012. Fabrication of ZnO nanoparticles confined in the channels of mesoporous carbon. Chem. Eng. J. 179, 388–393. https://doi.org/10.1016/j.cej.2011.10.087.

Tan, J., Li, W., Ma, C.H., Wu, Q., Xu, Z., Liu, S.X., 2018. Synthesis of honeycomb-like carbon foam from larch sawdust as efficient absorbents for oil spills cleanup and recovery. Materials 11, 1106–1117. https://doi.org/10.3390/ma11071106.

Tang, L.R., Huang, B., Yang, N.T., Li, T., Lu, Q.L., Lin, W.Y., Chen, X.R., 2013. Organic solvent-free and efficient manufacture of functionalized cellulose nanocrystals via one-pot tandem reactions. Green Chem. 15, 2369–2373. https://doi.org/10.1039/C3GC40965A.

Thines, K.R., Abdullah, E.C., Mubarak, N.M., Ruthiraan, M., 2017. Synthesis of magnetic biochar from agricultural waste biomass to enhancing route for waste water and polymer application: a review. Renew. Sustain. Energy Rev. 67, 257–276. https://doi.org/10.1016/j.rser.2016.09.057.

Van Oss, C.J., 2006. Interfacial Forces in Aqueous Media. CRC press, Boca Raton, New York. Wang, G.P., Zhang, L., Zhang, J.J., 2012. A review of electrode materials for electrochemical supercapacitors. Chem. Soc. Rev. 41, 797–828. https://doi.org/10.1039/C1CS15060J.

Wang, H.W., Yi, H., Zhu, C.R., Wang, X.F., Fan, H.J., 2015. Functionalized highly porous graphitic carbon fibers for high-rate supercapacitive electrodes. Nano Energy 13, 658–669. https://doi.org/10.1016/j.nanoen.2015.03.033

Wu, Q., Li, W., Tan, J., Liu, S.X., 2014. Flexible cage-like carbon spheres with ordered mesoporous structures prepared via a soft-template/hydrothermal process from carboxymethylcellulose. RSC Adv. 4, 61518–61524. https://doi.org/10.1039/C4RA12134A.

Wu, Q., Li, W., Tan, J., Wu, Y.J., Liu, S.X., 2015. Hydrothermal carbonization of carboxymethylcellulose: one-pot preparation of conductive carbon microspheres and water-soluble fluorescent carbon nanodots. Chem. Eng. J. 266, 112–120.

https://doi.org/10.1016/j.cej.2014.12.089.

Wu, Q., Gao, M.M., Cao, S.S., Hu, J.Q., Huang, L., Yu, S.T., Ragauskas, A.J., 2019. Chitosan-based layered carbon materials prepared via ionic-liquid-assisted hydrothermal carbonization and their performance study. J. Taiwan Inst. Chem. Eng. 101, 231–243. https://doi.org/10.1016/j.jtice.2019.04.039.

Xia, Y., Mokaya, R., 2004. Synthesis of ordered mesoporous carbon and nitrogen-doped carbon materials with graphitic pore walls via a simple chemical vapor deposition method. Adv. Mater. 16, 1553–1558. https://doi.org/10.1002/adma.200400391.

Xiao, L.P., Shi, Z.J., Xu, F., Runcang Sun, R.C., 2012. Hydrothermal carbonization of lignocellulosic biomass. Bioresour. Technol. 118, 619–623.

Yu, M., Han, Y.Y., Li, J., Wang, L.J., 2017. CO2-activated porous carbon derived from cattail biomass for removal of malachite green dye and application as supercapacitors. Chem. Eng. J. 317, 493–502. https://doi.org/10.1016/j.cej.2017.02.105.

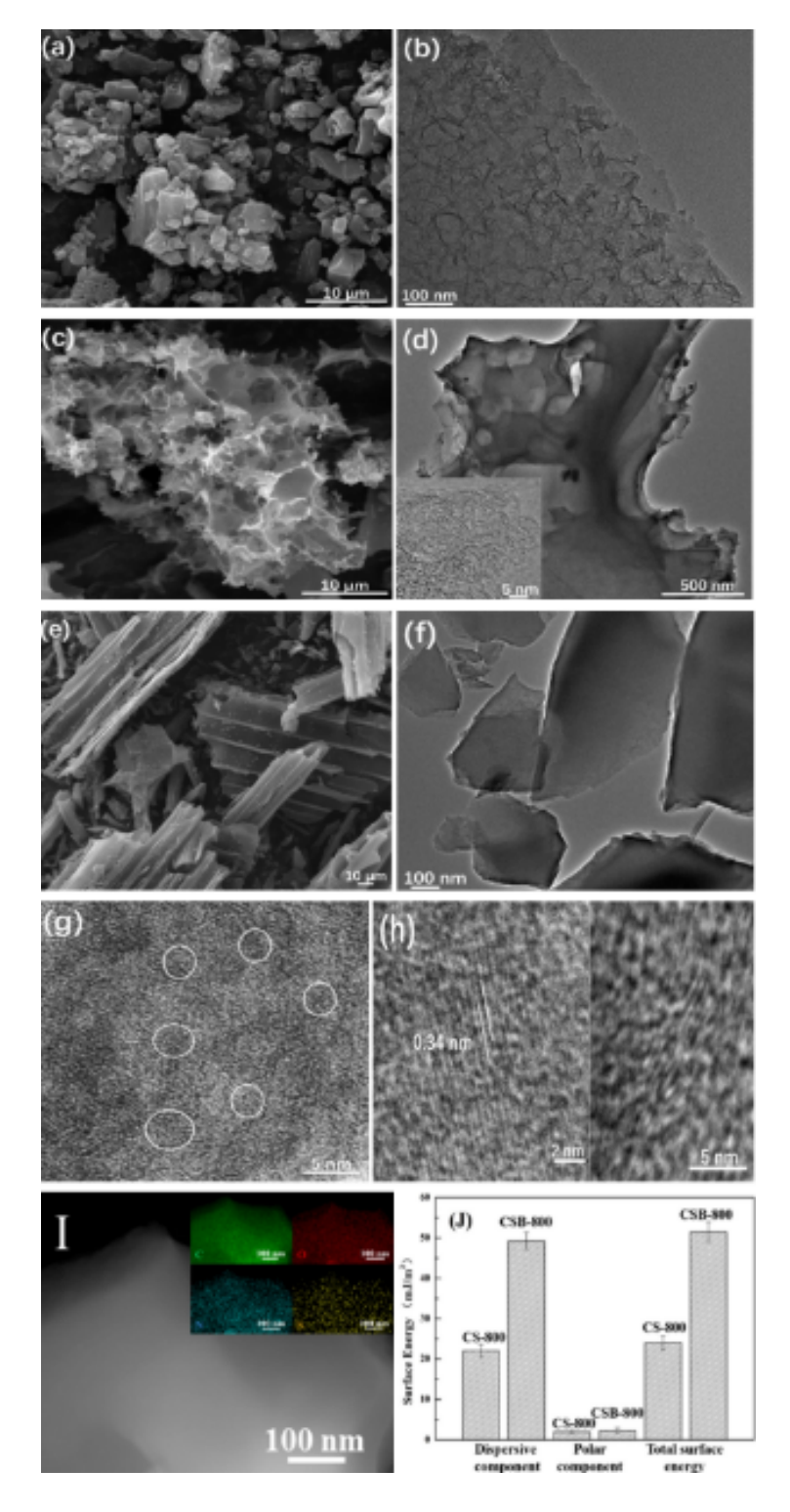


**Figure 1.** SEM and TEM images for (a, b) CSB-800, (c, d) CB-800, (e, f) CS-800, (g-h) HR-TEM of CSB-800, (I) corresponding EDX elemental mapping images of CSB-800 and (J) corresponding surface energy of CS-800 and CSB-800 calculated by contact angle test.

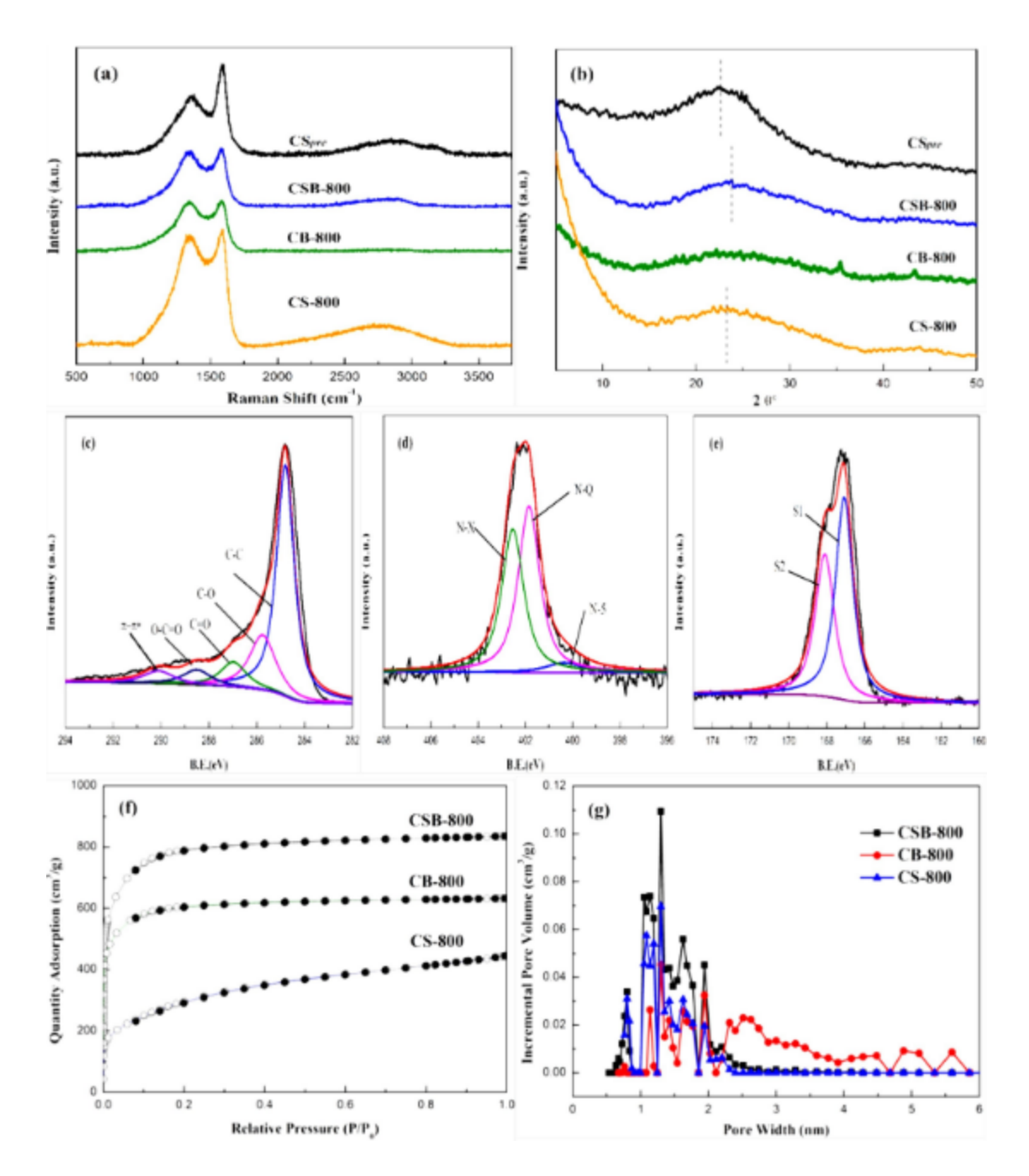


**Figure 2.** (a) Raman, (b) XRD test for  $CS_{pre}$ , CSB-800, CB-800 and CS-800, (c)  $C_{1s}$ , (d)  $N_{1s}$  and (e)  $S_{2p}$  high-resolution fitting peaks of CSB-800, (f) Nitrogen adsorption-desorption isotherms and (g) corresponding pore size distribution curves of CSB-800, CB-800 and CS-800.

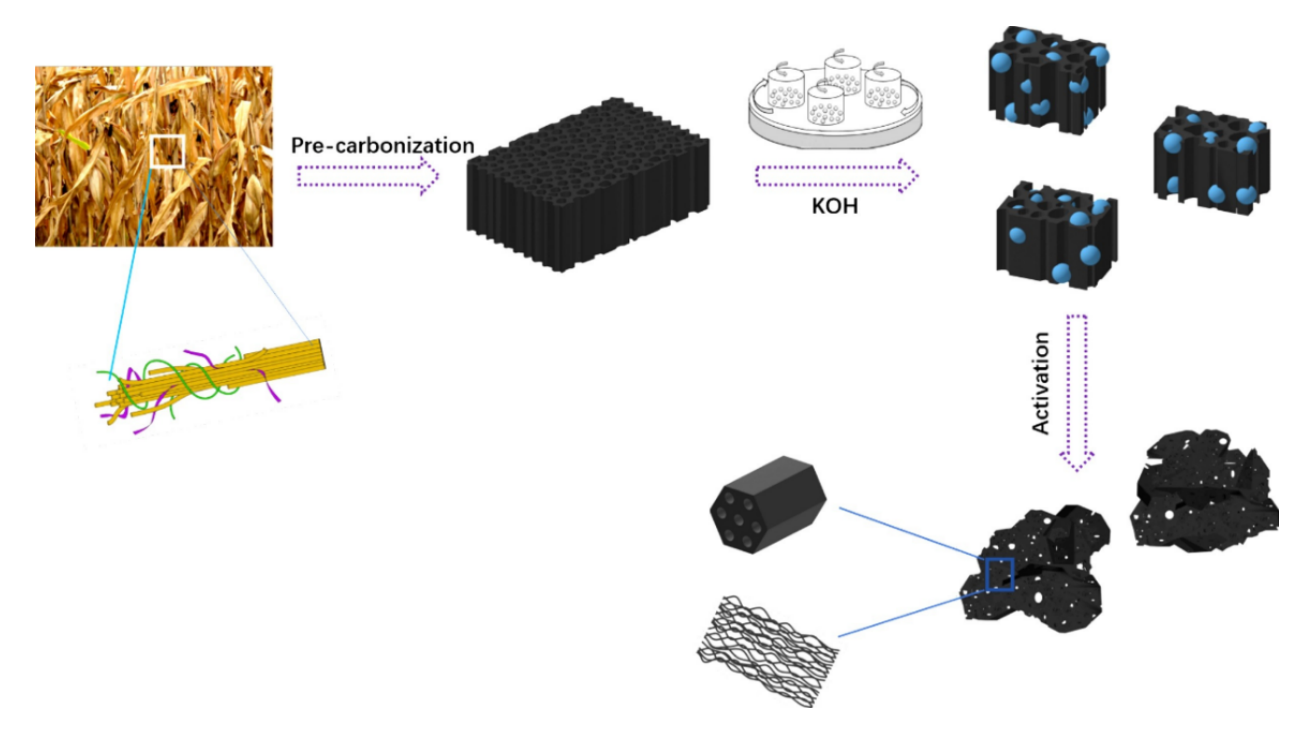


**Figure 3.** Proposed structural evolution process.

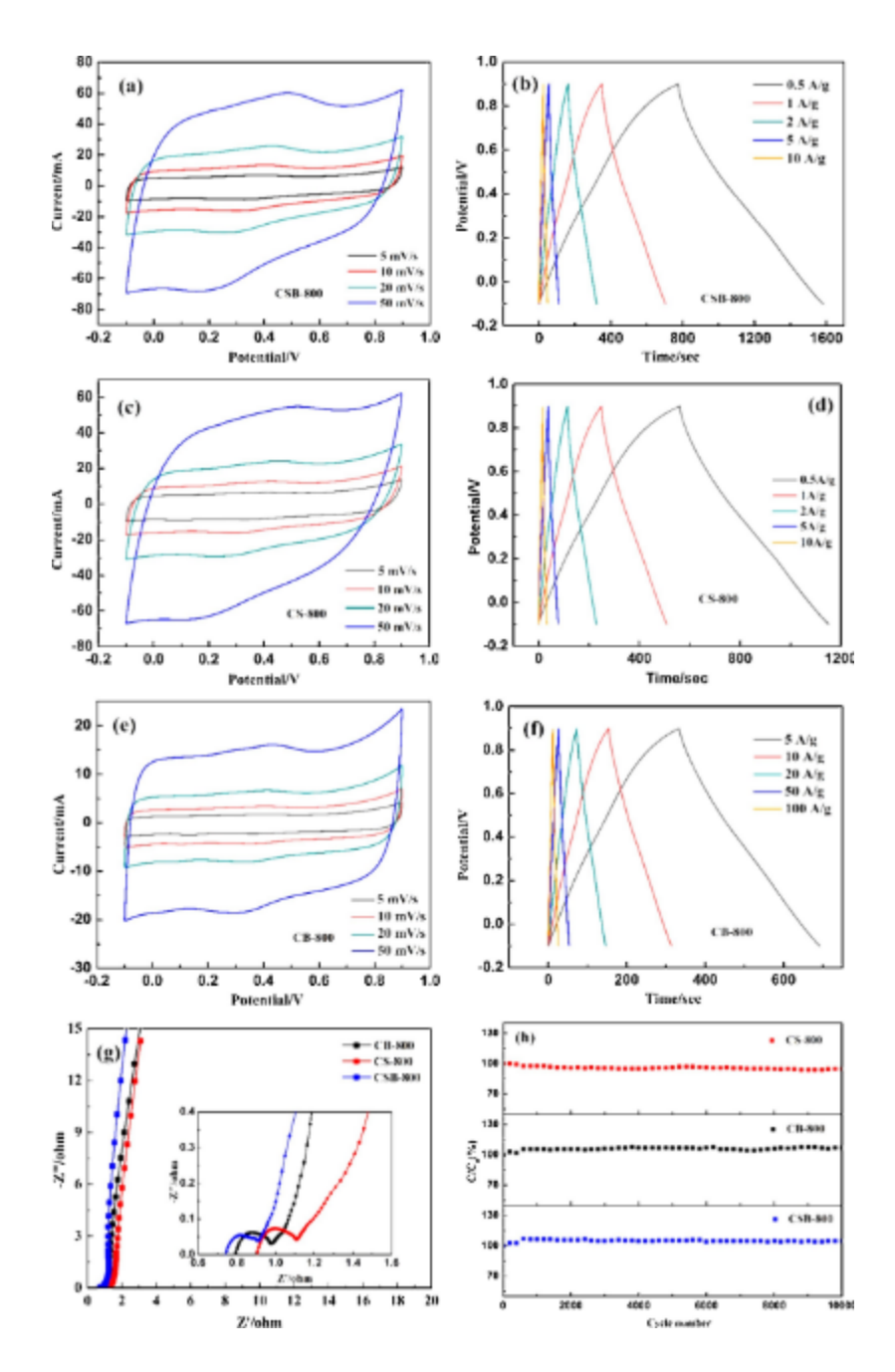


**Figure 4.** (a, c, e) CV curves at different scan rate, (b, d, f) GCD curves at different current densities, (g) Nyquist plots and (h) Cycle performance at 20 A/g for different samples in 1M H<sub>2</sub>SO<sub>4</sub> electrolyte.

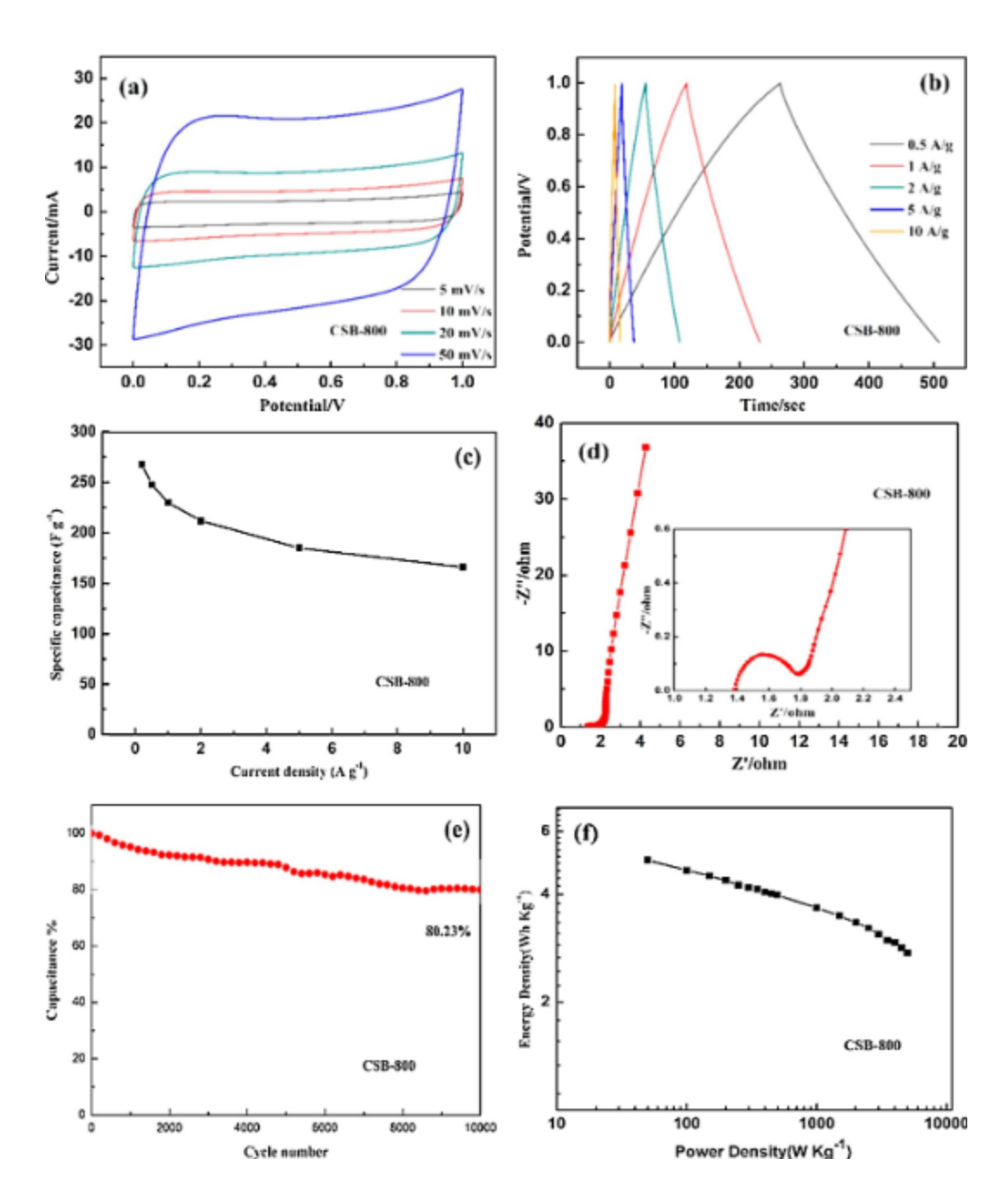


**Figure 5.** (a) CV curves at different scan rate, (b) GCD curves at different current densities, (c) Specific capacitance at different current densities, (d) Nyquist plots, (e) Cycle performance at 20 A/g and (f) Ragone plots of CSB-800 in two-electrode system.

 Table 1. Textural properties of obtained samples.

Name	S%a	N%a	C%a	O%a	Residual	Ash <sup>c</sup>	$I_D/I_G^d$
					carbon		
$CS_{pre}$	$5.3 \pm 0.2$	$8.9 \pm 0.2$	$66.3 \pm 0.5$	$19.4 \pm 0.2$	$82.3 \pm 0.4$	$2.3 \pm 0.1$	$1.58 \pm 0.01$
CSB-800	$4.6 \pm 0.1$	$9.2 \pm 0.2$	$69.6 \pm 0.4$	$16.4 \pm 0.2$	$88.8 \pm 0.7$	$0.9 \pm 0.1$	$1.66 \pm 0.01$
CB-800	$2.9 \pm 0.2$	$7.2 \pm 0.1$	$77.6 \pm 0.3$	$12.2 \pm 0.1$	$86.4 \pm 0.5$	$1.9 \pm 0.1$	$1.69 \pm 0.02$
CS-800	$2.9 \pm 0.1$	$5.6 \pm 0.2$	$79.1 \pm 0.5$	$12.4 \pm 0.1$	$87.5 \pm 0.4$	$2.3 \pm 0.1$	$1.92 \pm 0.02$

<sup>&</sup>lt;sup>a</sup> Tested by XPS.

<sup>&</sup>lt;sup>b</sup> Tested by TG with N<sub>2</sub>.

<sup>&</sup>lt;sup>c</sup> Tested by TG with Air.

<sup>&</sup>lt;sup>d</sup> Calculated by peak integral area.

 $\textbf{Table 2.} \ \, \textbf{Textural properties derived from the } \, N_2 \ \text{adsorption-desorption isotherms}.$ 

Samples	$S_{BET}$ (m <sup>2</sup> /g)	$S_{\text{meso}}$ (m <sup>2</sup> /g)	S <sub>micro</sub> (m <sup>2</sup> /g)	Pore Volume	Average pore
				$(cm^3/g)$	diameter (nm)
$CS_{pre}$	$135 \pm 12$	$133 \pm 10$	2 ± 1	$0.1 \pm 0.1$	$3.9 \pm 0.2$
CSB-800	$2441 \pm 105$	$927 \pm 73$	$1514 \pm 88$	$1.3 \pm 0.1$	$2.1 \pm 0.2$
CB-800	$1032 \pm 78$	$810 \pm 70$	$222 \pm 15$	$0.7 \pm 0.1$	$0.7 \pm 0.1$
CS-800	$1646 \pm 92$	$427 \pm 39$	$1220 \pm 81$	$1.0 \pm 0.1$	$2.1 \pm 0.2$